Biosynthesis of Silver/Silver Oxide Nanoparticles by Aqueous Leaves Extract of Mentha Piperita :The Effect of Silver Nitrate Concentration on the Product Type

Mohamed Bilal Goudjil[1], Souad Zighm[2], Djamila Hamada[3], Zineb Mahcene4 , Salah Eddine Bencheikh[5]

[1], [3], [5]Applied Sciences Faculty, Process Engineering Laboratory, Ouargla University, Ouargla 30000, Algeria.

Email: goudjil.bilal@univ-ouargla.dz

Email: djam2010ham@yahoo.fr

Email: bencheikh.salah@gmail.com

[2]Applied Sciences Faculty, Engineering Laboratory of Water and Environment in Middle Saharian Laboratory, Ouargla University, Ouargla 30000, Algeria.

Email: souad.zighmi@gmail.com

[3]Sciences of the nature and life Faculty, Protection of Ecosystems in Arid and Semi-Arid Zones Laboratory, Ouargla University, Ouargla 30000, Algeria.

Email: mahcene.zineb@gmail.com

Abstract

In this study, green synthesis of silver/ silver oxide nanoparticles (Ag/Ag2O NPs) was achieved by bio-reduction of silver nitrate using Mentha Piperita plant leaves extract. The effect of different silver nitrate concentrations on the nanoparticles' silver formation was studied. The obtained nanoparticles were characterized by UV-Vis, FT-IR, XRD and SEM techniques are used for this purpose. UV-Vis spectra showed maximum absorption in the range of 253–300 nm related to the silver. FTIR spectra exhibit a weak peak at 565 cm-1 attributed to silver NPs vibration, confirming the nanoparticles formation. The X-Ray Diffraction (XRD) analysis confirmed the crystalline nature of (Ag/Ag2O NPs) with an average size ranged in 31–42 nm. SEM showed that the green synthesizing silver nanoparticles having in general as cubical shape. As a result, the use of peppermint leaves extract offers its ease, fast, low cost and friendly to the environment compared to other methods.

Keywords: AgNO3 , Biomaterials, Green synthesis, Mentha Piperita, Nanoparticles, XRD.

I. Introduction

Medicinal plants are both a finished product for consumption and a raw material for obtaining bioactive substances that are at the origin of several modern medicines due to their richness in secondary metabolites, especially phenolic compounds with beneficial biological properties. Currently, the emergence of nanotechnology, which refers to the production at the nanometric scale (1 to 100 nm) of materials or products of controlled sizes and structures, is the consequence of the appearance of new physicochemical properties more advantageous and unique physicochemical properties that differ greatly from other materials due to the small size of the charges. These performances have contributed to radical changes in various fields of technology and science [1].

Plant products find imperative use in the synthesis of nanoparticles (NPs). Silver(Ag) is the metal of choice among noble metals for potential applications in biological systems, organic matter and medicine [2-4].

Among the plants with important pharmacological potentialities, Mentha piperita which is widely spread and used in Algeria. Their biological activities are closely linked to their richness in active substances, which they contain such as phenolic compounds.

In order to better understand the interest of bioactive substances of Mentha piperita, it seemed useful to us to undertake this present work which deals with the synthesis of silver nanoparticles using the extract of this plant.

In this study, green synthesis method was used which have emerged as a quick and simple approach to synthesis, inexpensive, environmentally friendly and cost-effective. we prepared silver nanostructures using different weight of silver nitrate directly in leaf extract solution and investigated their structural, morphological and optical properties.

1. Materials and Methods

A. Preparation of the leaf extract

The plant material that is used during the realization of this work consists of Mentha Piperita leaves

doi.org/10.31838/hiv23.03.49 Received: 19.10.22, Revised: 20.11.22, Accepted: 13.12.22.

species collected in March 2022 in the region of Tiaret (Western Algeria) coordinates (N 35.362222 °E 1.285555 °). Fresh leaves were washed and dried in a shade at room temperature for 5 days, and then crushed to obtain a fine powder. The extract was prepared by putting 40g of powder's leaves with 400ml of distilled water in a 500ml glass beaker. In addition, magnetic stirring at 350 rpm and heating at a temperature of 90°C is carried out for 1 hour. The extract was filtered using a filter paper (Whatman No: 2) and stored at 4°C for further use.

Synthesis of Silver nanoparticles by Mentha Piperita extract

Silver nanoparticles were synthesized by a modified protocol from previous researches [4-6]. Briefly, by adding with four different weight (0.1, 0.6, 0.9, and 1g) of the silver nitrate (AgNo3) to the 100 ml leaf extract in a 250 ml flask. AgNPs were immediately obtained with the reduction process. For one hour, the mixture was continuously stirred at 75 C. The transition from bright yellow to dark brown is an indication that silver nanoparticles are forming. The reasonable mechanism of silver nanoparticles formation may be due to the reduction of silver ions that takes place together with the phenolic compounds in the M. Piperita leaf extract.

Characterization of silver nanoparticles

Several techniques have been used for the characterization of silver nanoparticles such as: UV-Vis, FTIR, XRD and SEM and EDX

UV–Visible Spectroscopy

The device is the HACH DR6000 UV-Vis spectroscopy, which operates in the wavelength range of 190 to 1100 nm. The samples were analyzed in a quartz cell. The spectrophotometer enclosure is thermostated at 25°C and distilled water was used as reference solvent.

FTIR Spectroscopy

This technique was used to identify the functional groups present in a sample as well as the bonds developed after the formation of silver nanoparticles. The powder of silver nanoparticles prepared from leaf extract was deposited in the ATR (Attenuated Total Reflectance) spectroscopy.

X-ray Diffraction (XRD)

The structure and grain size of AgNPs were examined by XRD techniques using Xray diffractometer (BTX-716) with a Cu-Ka (k = 1.5406 A˚) in 2ϴ range of 5-70,whereas X-ray was generated with 30 kilovolts and at 20mA.

Scanning Electron Microscopy (SEM)

The surface morphology of all studied samples was observed by EVO-15 SEM (EVO 15, ZEISS, Germany) using an acceleration voltage of 15 kV supported with an energy dispersive X-ray Spectroscopy (EDX).

2. Results and discussion

Mentha Piperita-mediated synthesis of Ag/Ag2O NPs is more advantageous than chemical and physical synthesis because it is a clean, non-toxic, cost-effective, and environmentally friendly approach. In addition, Mentha Piperita is widely available in nature, making it a preferable plant material for industrial scaling up [7-9].

Phytochemical analysis of Mentha piperita leaf extract revealed that they contain polyphenols, flavonoids, tannins, and saponins [10, 11].

The color shift of the solution from yellow to dark brown in less than an hour is the most significant visual observation during the reaction. The production of Ag/Ag2O NPs is clearly indicated by the brown color. Based on this evidence, a possible mechanism for Ag2+ reduction and Ag/Ag2O NPs formation were proposed using Mentha piperita leaf extract.

During synthesis, plant leaf extracts that rich in polyphenol content are employed as bioreducing agents. The reduction process consists of transforming Ag2+ ions into Ag0. The Ag0 represented by the AgNPs is transformed into Ag/Ag2O NPs after annealing in the incinerator at 500°C for 2h [12].

B. UV–visible Spectroscopy

UV-Vis spectra of Ag/Ag2O nanoparticles synthesized using a peppermint extract are shown in Fig. 1. As can be seen in this figure, a maximum absorption peak is presented from the interval of 253 to 300 nm which gives a clue that silver/silver oxide nanoparticles may be formed [6, 13]. Moreover, the strong absorption peak can be caused by the collective oscillation of the electrons in the free conduction band which is excited by the incident electromagnetic radiation.

Furthermore, as seen, the samples' absorption intensity increased as the silver concentration increased. This shows that the amount of nanoparticles produced as a result of silver ion reduction has increased [14, 15].

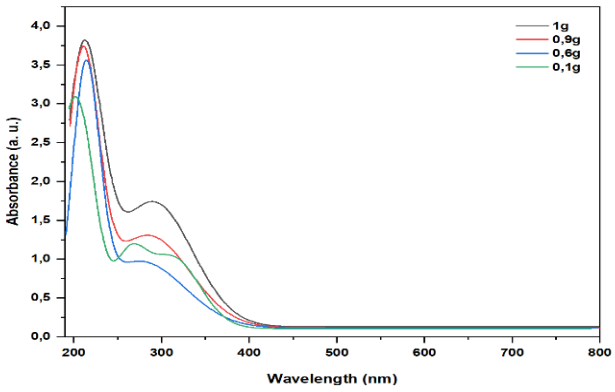

Fig. 1. UV–Vi's absorption spectrum of Silver nanoparticles synthesized

Estimation of the optical band gap:

Generally, the estimated optical energy band of a silver nitrate nanoparticle semiconductor (Eg) can be determined by extrapolation from the absorption band using the Tauc relation (Equation (1)) [16] :

$$(\alpha h\nu) = A(h\nu - E_g)^n \quad (1)$$

Where α is the absorption coefficient, A is constant, hv is the incident photon energy, and n is a constant depending on the nature of the electronic transition (n = 1/2 for indirect transition, n = 2 for direct transition as shown in Figure 2) , Eg is the optical band gap energy in electron-volts (eV) , and the exponent n = 1/2 for the direct allowed transition (Figure (2)) We obtained the energy gap from the intersection of the edge of the linear absorption part with the energy axis [17, 18].

Generally, several factors can affect the band gaps of prepared Ag/Ag2ONPs, i.e., crystallinity, crystallite size, particle size, particle shape and composition [19]. Low band gap energies allow Ag/Ag2ONPs to absorb the vast majority of the solar spectrum, and direct band gaps give Ag/Ag2ONPs a large absorption coefficient.

As shown in Table 1, the AgNo3 concentration increases from 0.1g to 1g reflect that both direct bandgap decreases from 5.29 to 4.98 eV, and the indirect bandgap decreases from 2.95 to 2.65 eV.

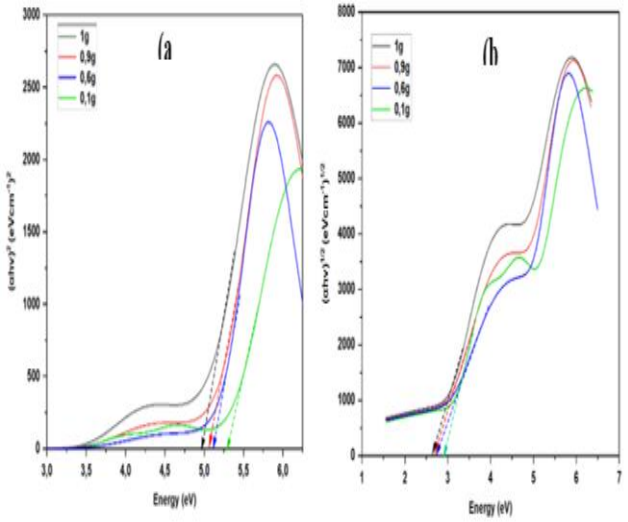

Fig. 2. Determination of optical energy gap for (a) direct and (b) indirect bandgaps transition using Tauc's method.

The results are consistent with the literature review that the bandgap decrease with a increases in concentration [20, 21].

C. Estimation of the Urbach energy

The Urbach energy is also known as the Urbach tail and can be detected by the UV-vis spectra. The highest value of Urbach energy shows lower crystallinity and disorder in Ag/Ag2O NPs. The Urbach energy Eu is derived by taking the mutual values of the slopes of the linear part of ln(a) as a function of photon energy (Fig. 3) [22]

$$\ln a = \frac{hv}{Eu} + constant\ (\ln a_0) \quad (2)$$

The estimated Urbach energy values for the samples are presented in Table 1. The results indicated that the Urbach energy of the Ag/Ag2O NPs slightly decreases from 0.67 to 0.36 eV with the increase in the particle size and the increase in silver nitrate concentrations. These results were explained for Urbach energy due to the effect of structural and thermal perturbation.

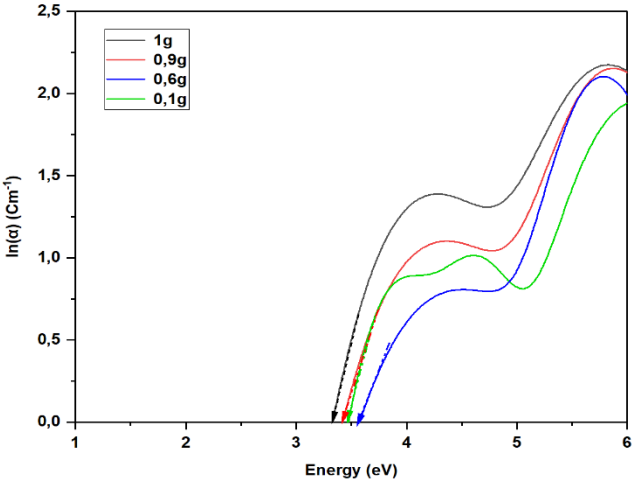

Fig. 3. Urbach energy estimate of the silver nitrate nanoparticles synthesized by the extract of Mentha piperita leaf

Table 1 The values of direct band gap, indirect band gap and Urbach energy of the biosynthesized Ag/Ag2O.

Samples	Direct Optical band gap (eV)	Indirect Optical band gap (eV)	Urbach energy (eV)
0.1g	5,29	2,95	0,666
0.6g	5,12	2,79	0,502
0.9g	5,05	2,70	0,436
1g	4,98	2,65	0,364

Fourier Transform Infrared spectroscopy (FTIR)

The FT-IR analysis was used for both Mentha Piperita leaf extract and synthesized silver nanoparticles solution before annealing at 500°C to identify the possible biomolecules responsible for Ag/Ag2O Nps synthesis.

The study was carried out by FTIR spectrophotometer (Cary670) in the frequency range 4000- 400 cm-1 for Mentha Piperita leaf extract with different spectra of nanoparticles prepared with different ration (Figure 4). The result of FTIR spectrum exhibited several absorption bands that correspond to the functional groups of the biomolecules existing in the plant extract. Main absorption peaks were observed at 3300, 2900, 1740, 1606, 1417, 1026 and 565 cm-1. The broadband, at 3300 cm-1, is due to the OH group stretching vibration. Significant peaks were found at (2960 ,2871) cm-1 ascribed to the C-H of methyl group, the absorption peaks situated around 1740 and 1417 cm-1 correspond to the stretching vibrations of C=C, C-C, and C-O of the aromatic's cycles. The peak located at 1026 are assigned to the

stretching band of C-O. Weak bands at 565 cm-1 silver nanoparticles solution before annealing indicate to the Ag-O stretching band of Ag/Ag2O Nps [23-25].

The comparison between the IR spectra of Mentha Piperita extract before and after the addition of silver nitrate shows that:

A decrease in the intensity of the broad band from 3300 cm-1 to 2900 cm-1 which represent the free OH groups in the molecule, , this group reacts to reduce Ag+ in reaction media which leads to the formation silver nanoparticles according to several authors [26-28]

An appearance of a 1740 cm-1 peak is observed corresponding to the(C=O) grouping.

Also, an appearance peak is observed at 565 cm-1 attributed to the Ag/Ag2O Nps binding of silver nitrate.

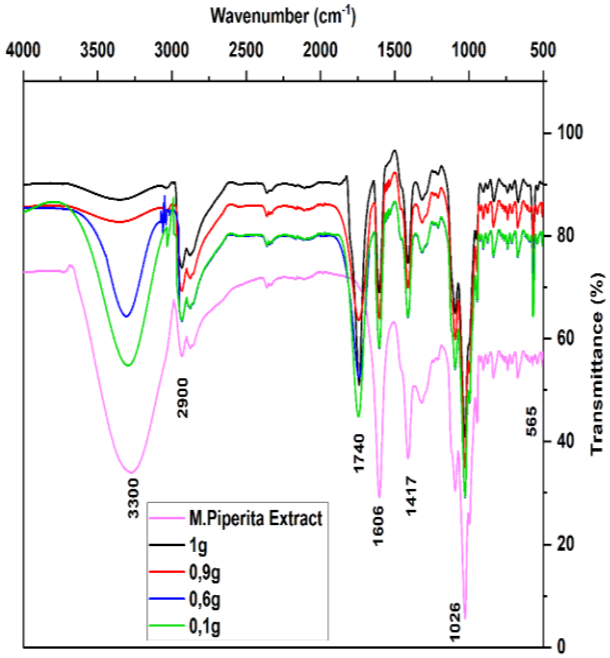

Fig. 4. FT-IR spectra of M. Piperita leaf extract and as synthesized silver nanoparticles solution before annealing with different silver nitrate concentration.

A. Crystal structure and crystallite size

XRD patterns of synthesized AgNPs Prepared using the Mentha Piperita leaf extract and various concentrations of silver nitrate after annealing at 500°C are shown in Figure 5.

The diffractogram affirms the existence of two crystalline phases, Silver (Ag) and Silver oxide (Ag2O). The peaks position with 2θ values of 38.3°, 44.45° and 63.95° corresponding to the crystalline planes of (111), (200) and (220) which confirm the formation of the face-centered cubic structure [29, 30] ((ICSD) Card No. 98-005-3759).

The other seven characteristic peaks at 2θ values of 26.09°, 32.09°, 37.23°, 46.03°, 53.67°, 63.92° and 67.13° are attributed to the crystal planes of (110), (111), (200), (211), (220), (311) and (222) which correspond to the face-centered cubic structure of silver (I) oxide [31] ((ICSD) Card No. 98-017-4092).

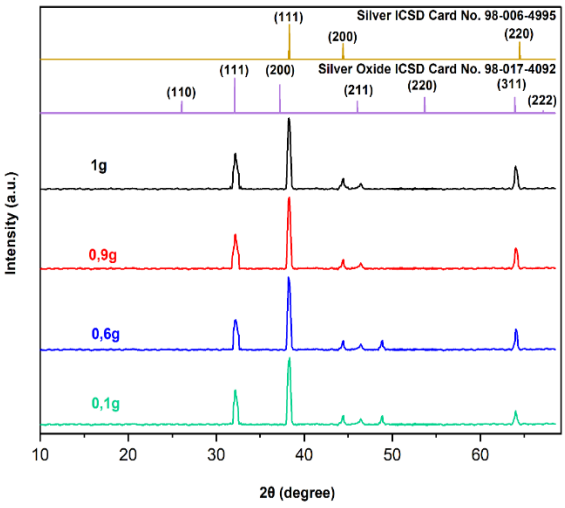

Fig. 5. XRD patterns of Silver/Silver Oxide nanoparticles synthesized

Using the Scherrer formula Eq (3), the average crystallite size of the synthesized nanoparticles was determined by choosing the peaks at 2θ values:

$$D = \frac{K\lambda}{\beta \cos\theta} \quad (3)$$

Where D is the crystalline size (nm), β is the full width at half maximum of the diffraction peak (FWHM) of the most intense diffraction peak, λ the X-ray wavelength (1.5406 Å) and θ is the Bragg angle of diffraction [32].

Table 2 displays the influence of different concentration on Ag/Ag2O crystallite size. The findings demonstrated that the concentration ratio has an impact on crystallite size. Noteworthy that the Ag/Ag2O NPs crystallite size was unaffected by the concentration ratio's increase from 0.9 to 1g. On the other hand, the crystallite size of Ag/Ag2O considerably fell from 42.52 nm to 34.78 nm when the concentration ratio increased from 0.6 to 0.9g.

Numerous earlier research [33-35] also revealed that reducing the crystallite size by increasing the ratio of surfactant (plant extract) was possible.

B. Scanning Electron Microscopy (SEM)

The formation of Ag/Ag2O NPs and their morphological dimensions were studied using the SEM. Fig. 6 (a–d) exhibits SEM images of the synthesized silver (Ag/Ag2O NPs). It is observed that most of them are cubic in nature and irregular shaped. Further analysis of silver nanoparticles, by EDAX, as shown in (Fig.6 (4e)) its associated data, confirms the presence of silver and oxygen, with the weight percentage of about 68.84% Ag and 3.53% O. Results means that most of the particles formed are specific to AgNPs.

3. Conclusion

A simple, one-step green approach was devoted for the synthesis of AgNPs. The prepared Ag/Ag2O NPs product has a cubical structure with an average diameter is 31.96-42.52 nm. Results showed the variation of the weight Ag precursor allows us to

strictly control the size and shape of the silver nanoparticles, which could be a potential source for the production of highly efficient antioxidant coatings.

4. Acknowledgment

Authors are grateful to the Center for Scientific and Technical Research in Physico-Chemical Analysis Ouargla (C.R.A.P.C), Laboratory of Sahara Geology and Laboratory of Dynamics, Interaction and Reactivity of Systems Ouargla for their great contribution in the realization of this work.

5.

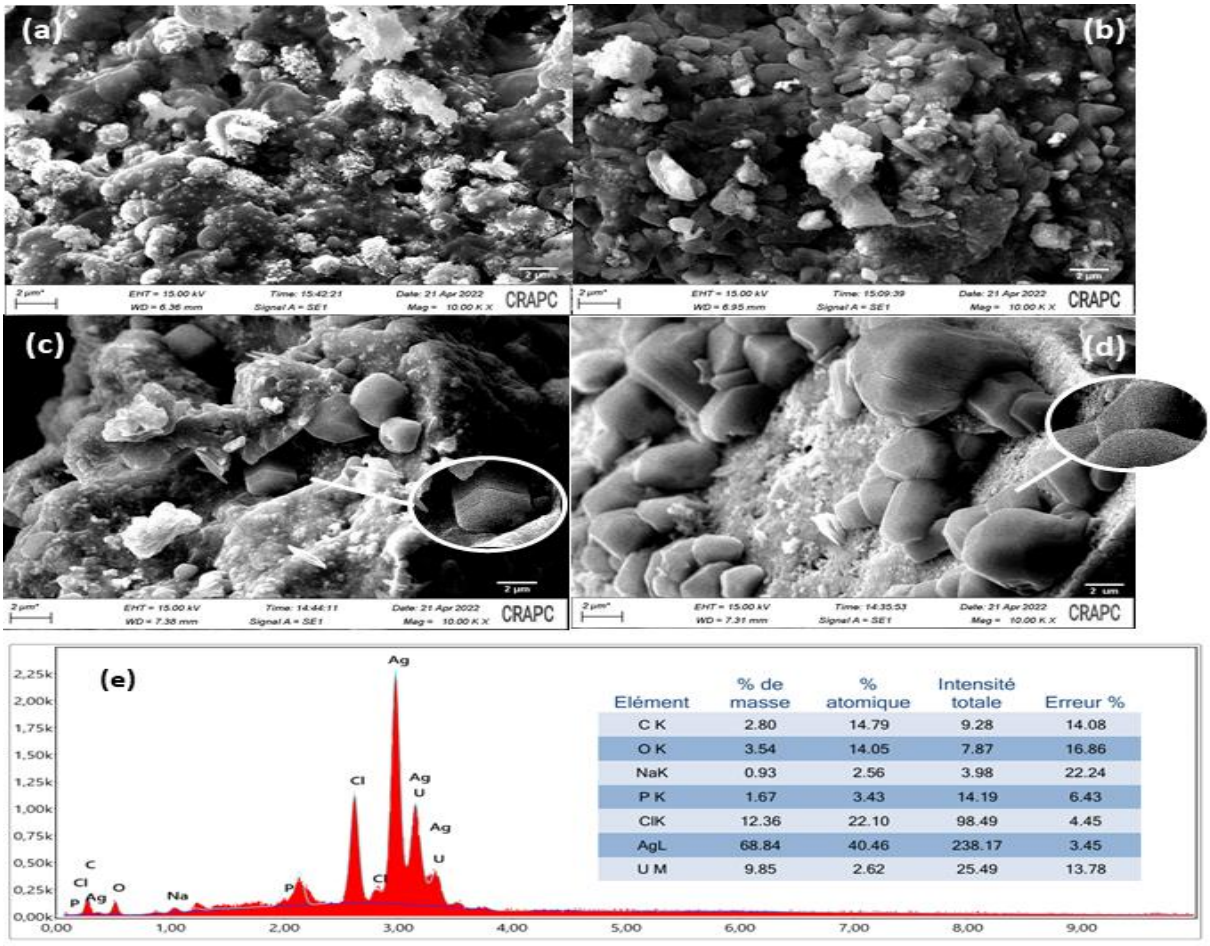

Elément	% de masse	% atomique	Intensité totale	Erreur %
C K	2.80	14.79	9.28	14.08
O K	3.54	14.05	7.87	16.86
NaK	0.93	2.56	3.98	22.24
P K	1.67	3.43	14.19	6.43
ClK	12.36	22.10	98.49	4.45
AgL	68.84	40.46	238.17	3.45
U M	9.85	2.62	25.49	13.78

Fig. 6. SEM images of green synthesized Ag /Ag_2O NPs nanoparticles: a) 0.1 g, b) 0.6 g, c) 0.9 g, d) 1 g and e) EDAX of silver nanoparticles

References

[1] Ramsden, J., Nanotechnology: an introduction. 2016: William Andrew.

[2] Nascimento, J., et al., New advances of the nanotechnology in textile engineering: functional finishing with quantum dots and others nanoparticles, in Nanomaterials and Nanotechnology. 2021, Springer. p. 239-281.

[3] Singh, S., P. Rajesh, and Y. Ravindra, Study And Evaluation Of The Microorganisms For The Formation Of Metal Nanoparticles And Their Application. Journal of Positive School Psychology, 2022: p. 4425-4433.

[4] Oves, M., et al., Green synthesis of silver nanoparticles by Conocarpus Lancifolius plant extract and their antimicrobial and anticancer activities. Saudi Journal of Biological Sciences, 2022. 29(1): p. 460-471.

[5] Anandalakshmi, K., J. Venugobal, and V. Ramasamy, Characterization of silver nanoparticles by green synthesis method using Pedalium murex leaf extract and their antibacterial activity. Applied Nanoscience, 2016. 6(3): p. 399-408.

[6] Bouafia, A. and S.E. Laouini, Green synthesis of iron oxide nanoparticles by aqueous leaves extract of Mentha Pulegium L.: Effect of ferric chloride concentration on the type of product. Materials Letters, 2020. 265: p. 127364.

[7] Uribe, E., et al., Assessment of vacuum-dried peppermint (Mentha piperita L.) as a source of natural antioxidants. Food chemistry, 2016. 190: p. 559-565.

[8] Masłowski, M., et al., Potential application of peppermint (Mentha piperita L.), german chamomile (Matricaria chamomilla L.) and yarrow (Achillea millefolium L.) as active fillers in natural rubber biocomposites. International Journal of Molecular Sciences, 2021. 22(14): p. 7530.

[9]Jurić, T., et al., The evaluation of phenolic content, in vitro antioxidant and antibacterial activity of Mentha piperita extracts obtained by natural deep eutectic solvents. Food Chemistry, 2021. 362: p. 130226.

[10] KS, S. and S. Shinde, Phytochemical screening and evaluation of In-vitro antimicrobial properties of

Mentha piperita L. Int J Life Sci, 2019. 7: p. 785-790.
[11] Mainasara, M.M., et al., Comparison of phytochemical, proximate and mineral composition of fresh and dried peppermint (Mentha piperita) leaves. Journal of Science and Technology, 2018. 10(2).
[12] Barhoum, A., et al., Chapter 20 - Recent trends in nanostructured particles: synthesis, functionalization, and applications, in Fundamentals of Nanoparticles, A. Barhoum and A.S. Hamdy Makhlouf, Editors. 2018, Elsevier. p. 605-639.
[13] Zare, M., et al., Novel Green Biomimetic Approach for Synthesis of ZnO-Ag Nanocomposite; Antimicrobial Activity against Food-borne Pathogen, Biocompatibility and Solar Photocatalysis. Scientific Reports, 2019. 9(1): p. 8303.
[14] Naika, H.R., et al., Green synthesis of CuO nanoparticles using Gloriosa superba L. extract and their antibacterial activity. Journal of Taibah University for Science, 2015. 9(1): p. 7-12.
[15] Kumar, B., et al., Andean Sacha Inchi (Plukenetia Volubilis L.) leaf-mediated synthesis of Cu2O nanoparticles: a low-cost approach. Bioengineering, 2020. 7(2): p. 54.
[16] Strehlow, W. and E.L. Cook, Compilation of energy band gaps in elemental and binary compound semiconductors and insulators. Journal of Physical and Chemical Reference Data, 1973. 2(1): p. 163-200.
[17] Jayaprakash, P., M.P. Mohamed, and M.L. Caroline, Growth, spectral and optical characterization of a novel nonlinear optical organic material: d-Alanine dl-Mandelic acid single crystal. Journal of Molecular Structure, 2017. 1134: p. 67-77.
[18] Mallick, P. and B. Dash, X-ray diffraction and UV-visible characterizations of α-Fe2O3 nanoparticles annealed at different temperature. Nanosci. Nanotechnol, 2013. 3(5): p. 130-134.
[19] Yang, Y., et al., Cu2O/CuO bilayered composite as a high-efficiency photocathode for photoelectrochemical hydrogen evolution reaction. Scientific reports, 2016. 6(1): p. 1-13.
[20] Gaffar, M., A.A. El-Fadl, and S.B. Anooz, Influence of strontium doping on the indirect band gap and optical constants of ammonium zinc chloride crystals. Physica B: Condensed Matter, 2003. 327(1): p. 43-54.
[21] Liu, D., et al., Indirect-to-direct band gap transition and optical properties of metal alloys of Cs 2 Te 1− x Ti x I 6: a theoretical study. RSC advances, 2020. 10(60): p. 36734-36740.
[22] Martienssen, W., Über die excitonenbanden der alkalihalogenidkristalle. Journal of Physics and Chemistry of Solids, 1957. 2(4): p. 257-267.
[23] Masikini, M., The use of cyclodextrin template-based metal oxide nanomaterials in the development of electrochemical sensors for phenolic endocrine disruptor compounds. 2010, University of the Western Cape.
[24] Pawar, O., et al., Green synthesis of silver nanoparticles from purple acid phosphatase apoenzyme isolated from a new source Limonia acidissima. Journal of Experimental Nanoscience, 2016. 11(1): p. 28-37.
[25] Yassin, M.T., et al., Facile Green Synthesis of Silver Nanoparticles Using Aqueous Leaf Extract of Origanum majorana with Potential Bioactivity against Multidrug Resistant Bacterial Strains. Crystals, 2022. 12(5): p. 603.
[26] Djamila, B., et al., In vitro antioxidant activities of copper mixed oxide (CuO/Cu2O) nanoparticles produced from the leaves of Phoenix dactylifera L. Biomass Conversion and Biorefinery, 2022: p. 1-14.
[27] Abdullah, J.A.A., et al., Green synthesis and characterization of iron oxide nanoparticles by pheonix dactylifera leaf extract and evaluation of their antioxidant activity. Sustainable Chemistry and Pharmacy, 2020. 17: p. 100280.
[28] Bouafia, A., et al., Green biosynthesis and physicochemical characterization of Fe3O4 nanoparticles using Punica granatum L. fruit peel extract for optoelectronic applications. Textile Research Journal, 2022. 92(15-16): p. 2685-2696.
[29] Kohan Baghkheirati, E., et al., Synthesis and antibacterial activity of stable bio-conjugated nanoparticles mediated by walnut (Juglans regia) green husk extract. Journal of Experimental Nanoscience, 2016. 11(7): p. 512-517.
[30] Meng, Y., A sustainable approach to fabricating Ag nanoparticles/PVA hybrid nanofiber and its catalytic activity. Nanomaterials, 2015. 5(2): p. 1124-1135.
[31] Rajabi, A., et al., Development and antibacterial application of nanocomposites: Effects of molar ratio on Ag2O–CuO nanocomposite synthesised via the microwave-assisted route. Ceramics International, 2018. 44(17): p. 21591-21598.
[32] Klug, H.P. and L.E. Alexander, X-ray diffraction procedures: for polycrystalline and amorphous materials. 1974.
[33] Moya, C., X. Batlle, and A. Labarta, The effect of oleic acid on the synthesis of Fe 3− x O 4 nanoparticles over a wide size range. Physical Chemistry Chemical Physics, 2015. 17(41): p. 27373-27379.
[34] Dehsari, H.S., et al., Effect of precursor concentration on size evolution of iron oxide nanoparticles. CrystEngComm, 2017. 19(44): p. 6694-6702.
[35] Laouini, S., A. Bouafia, and M. Tedjani, Catalytic activity for dye degradation and characterization of silver/silver oxide nanoparticles green synthesized by aqueous leaves extract of Phoenix dactylifera L. 2021.